RSC Advances

ROYAL SOCIETY OF CHEMISTRY

www.rsc.org/advances

Journal Name

ARTICLE

Graphene oxide-assisted preparation of poly(vinyl alcohol) /Carbon Nanotube/reduced graphene oxide nanofibers with high carbon content by electrospinning technology†

Received 00th January 20xx,
Accepted 00th January 20xx

DOI: 10.1039/x0xx00000x

www.rsc.org/

Song Yao, Yanbao Li*, Zhihang Zhou and Haichen Yan

In this article, the poly(vinyl alcohol) (PVA) based nanofibers with high carbon content were prepared via the electrospinning technology. Graphene oxide (GO) was used as the dispersing agent to improve the dispersion of multi-walled carbon nanotubes (MWCNTs) in the electrospinning solution and the PVA based nanofibers, and as the precursor of graphene. The microstructure of the PVA/GO/MWCNTs nanofibers were examined via the field emission scanning electron microscopy (FESEM) and transmission electron microscopy (TEM). The FESEM/TEM results show that MWCNTs were dispersed well in PVA matrix along with assistance of GO. The stability of the PVA/GO/MWCNTs nanofiber mat in aqueous solution is provided via the crosslinking network after crosslinked with glutaraldehyde (GA). Then, the PVA/RGO/MWCNTs nanofiber mat was obtained by reduction of GO after the crosslinked PVA/GO/MWCNTs nanofiber mat was soaked into hydrazine hydrate solution. The I_D/I_G value of GO in nanofibers increases from 0.83 to 1.11 after reduction via hydrazine hydrate at 95 °C for 1 h (hour), which indicates that the reduction of GO does take place . After addition of GO, the tensile strength of the PVA nanofiber mat decreases from 16.7±0.7 MPa to 13.2±0.8 MPa. After addition of MWCNTs, the tensile strength of the PVA/GO nanofiber mat increases from 13.2±0.8 MPa to 18.1±0.5 MPa. At the same time, the crosslinking network enhances the tensile strength of these nanofiber mats as well. The volume conductivity of the PVA nanofiber mat increases from $5.11\pm0.96\times10^{-11}$ S/m to $2.33\pm0.20\times10^{-7}$ S/m when the carbon content in the PVA based nanofibers reaches to 21 wt%.

Introduction

In the past few years, the electrospinning technology, the extraordinary simple and versatile method to prepare ultra-fine fibers from solution, has attracted considerable attentions. The different nonwoven nanofiber mats prepared by the electrospinning technology have been widely applied in many fields such as biomedical applications,[1, 2] filtration,[3] and electrical or electronic fields[4, 5]. Their electrical or electronic applications have been investigated intensively because the electrospinning technology has advantage of low-cost production for small electronic devices and sensors.[6, 7] Generally, in order to achieve high performance in electrical application, the electrospinning polymer solution should be mixed with conductive fillers.

Carbon nanotubes (CNTs) have some excellent properties such as electrical and mechanical properties.[8] The CNTs-filled nanofibers own a wide range of application such as in filters,[9] sensors,[10] thermal interface materials,[11] drug delivery[12]. The inclusion of CNTs in nanofibers will improve the specific properties of the nanofibers. Shoushtari et al[13] reported introduction of multi-walled carbon nanotubes (MWCNTs) can improve reflection loss of poly(vinyl alcohol) (PVA) nanofibers applied in the field of microwave absorption. Jeong et al[14] added MWCNTs into the electrospun PVA nanofibers to enhance their tensile strength. Ding et al[15] reported that the electrical conductivity of the PVA based films can be improved obviously from 1.2×10^{-5} S/cm to 3.6×10^{-4} S/cm by inclusion of MWCNTs.

To obtain the specific properties, CNTs must be dispersed uniformly in nanofibers. Unfortunately, serious aggregation can be easily found in the CNTs/polymer composites due to the strong van der Waals force between the nanotubes of CNTs.[16, 17] The mechanical, electrical and other properties of the CNTs-filled nanofibers are deteriorated due to the aggregation of CNTs. So CNTs should be treated appropriately to avoid their aggregation in nanofibers. Recently, many treatment methods have been employed to improve the dispersion of CNTs in composite system.[18-20] For example, Kim et al[18] obtained the stabilized dispersion of CNTs in aqueous solution after chemical oxidization of CNTs in a mixture of sulfuric acid and nitric acid (3:1 in volume ratio) under ultrasonic treatment. Wang et al[19] prepared a well dispersed CNTs solution by combination of microwave treatment and acid oxidation. Kim et al[20] improved dispersion stability of CNTs in aqueous solution by graft of poly(ethylene glycol) (PEG) chain on their surfaces. Among these treatment

College of Materials Science and Engineering, Nanjing Tech University, Nanjing 210009, China. E-mail: lyanbao@163.com, ybli@njtech.edu.cn; Fax: +86-25-83587260; Tel: +86-25-83587260

† Electronic supplementary information (ESI) available.

methods, it is worthy to note that graphene oxide (GO) disperses CNTs in aqueous solution.[21] Many researchers have prepared some composites filled by CNTs through GO-assisted dispersion.[22-25] However, nobody has employed this method to prepare the electrospun nanofibers. So this may be a good attempt to prepare the electrospun CNTs-filled nanofibers via GO-assisted dispersion of CNTs.

As a precursor of chemically converted graphene, GO can be readily prepared by exfoliation of oxidized graphite. GO contains plenty of functional groups, such as hydroxyl, epoxy, ketone and carboxyl, which randomly assemble at edge and basal plane.[26] These functional groups make GO sheets possess strong hydrophilicity. However, GO sheet consists of aromatic regions with unoxidized benzene rings, which can form π-π stacking interaction with other aromatic molecules.[22] CNTs consist of hollow cylindrically wrapped graphene sheets which own a lot of aromatic regions.[27] Therefore, CNTs can be well dispersed in composite solution with assistance of GO through the interaction of π-π stacking between GO and CNTs.

Although there are many methods for dispersing CNTs well in composite material, it is difficult to obtain the electrospun nanofibers with high carbon content because a large amount of CNTs lead to their serious aggregation in nanofibers.[28, 29] Herein, in order to solve this problem, GO was used as a dispersing agent to improve the dispersion of MWCNTs in PVA based nanofibers. After reduction of GO in the PVA/GO/MWCNTs nanofibers, the carbon content in nanofibers reaches to 21 wt%.

Experimental

Materials

PVA was purchased from Shanghai Yingjia Industrial Development Co., Ltd (degree of polymerization 2400±50; degree of hydrolysis 88%). Multi-walled carbon nanotubes (MWCNTs) were provided by Chengdu Organic Chemicals Co., Ltd. Graphite powders, ethanol, hydrogen peroxide (H_2O_2, 30.0%) and glutaraldehyde (GA, 25% aqueous solution) were purchased from Sinopharm Chemical Reagent Co., Ltd. Methylbenzene, sulphuric acid (H_2SO_4, 98.0%), potassium permanganate ($KMnO_4$, 99.9%), hydrochloric acid (HCl, 37.0%) and hydrazine hydrate (80% aqueous solution) were purchased from Shanghai Lingfeng Chemical Reagent Co., Ltd. Sodium nitrate ($NaNO_3$) was purchased from Xilong Chemical Co. Ltd. All reagents are analytical grade without further purification.

Preparation of GO

GO was synthesized by Hummers' method from graphite powders. In this method, H_2SO_4 (46 ml) was poured into a three-neck flask and cooled to 0 ^oC. Graphite powders (1 g) and $NaNO_3$ (1 g) were mixed with the cooled H_2SO_4. The mechanical stirring was employed throughout the preparation process of GO. $KMnO_4$ (6 g) was added slowly into the mixed suspension after stirring for 30 min. The mixture reacted at 20 ^oC for 0.5 h (hour) and the temperature of mixture was kept at 35 ^oC for 1 h. After that, 92 mL deionised water was added slowly into the mixture, and then the temperature was kept at 100 ^oC for 15~20 min. H_2O_2 (30%, 5 mL) was used to remove the residual $KMnO_4$ after diluting the mixture with 150 mL deionised water. The filter cake was obtained after filtration and then washed with 5 wt% HCl aqueous solution to remove the ions. For purification, the filter cake was washed with deionised water and centrifuged for several times. Finally, the GO solution was obtained after exfoliation of the graphite oxide by ultrasonic treatment.

Preparation of the nanofiber mats

PVA solution was prepared by dissolution of 1.4 g PVA into 20 mL deionised water under constant stirring at room temperature for 2 d (days). The PVA/GO solution was prepared by dissolution of 1.4 g PVA into 20 mL GO solution (5 mg/mL) under constant stirring at room temperature for 2 d. For the preparation of PVA/GO/MWCNTs mixed solution, 0.2 g MWCNTs were dispersed in 20 mL PVA aqueous solution by ultrasonic treatment for 30 min. Afterward, 0.1 g GO was added to the mixed solution after ultrasonic treatment for 15 min. Thereby, an uniform, stable PVA/GO/MWCNTs solution was achieved via using GO as dispersing agent. Finally, 1.3 g PVA was dissolved in the mixed solution so that a composite solution of suitable viscosity could be obtained for electrospinning.

A home-made electrospinning apparatus was utilized in this article. The tip (gauge 24) of syringes was connected to a direct current high-voltage generator (DW Co., Ltd. Tianjing China) with a wire. The electrospinning solution was loaded into a 5 mL disposable syringe. The flow rate was controlled in a range of 20~25 μL/min with a syringe pump (Longer Pump Co., Ltd. Baoding China). The applied voltage was 13 kV between the tip of the stainless needle and the grounded aluminium foil collector. The distance between the spinneret and the collector was 15 cm.

Crosslinking of the nanofiber mats

Acid methylbenzene (30 mL, pH=2~3, adjusted by HCl solution) was poured into a separatory funnel. Glutaraldehyde (GA) (3 mL) as crosslinked agent was mixed with acid methylbenzene. Then the upper turbid solution was obtained through the separatory funnel. These nanofiber mats were placed in the glutaraldehyde-methylbenzene solution. Afterwards, the crosslinked nanofiber mats were collected after reaction for 4 h at room temperature and washed with ethanol and water, alternatively, for three times to remove methylbenzene. Finally, the crosslinked nanofiber mats were dried at room temperature.

Reduction of GO in the nanofibers

The crosslinked nanofiber mats were soaked into 200 mL mixed solution of deionised water and hydrazine hydrate (0.12 mL, 80 wt%) at 95 ^oC for 1 h. In order to remove the residual hydrazine hydrate, these nanofiber mats were washed with deionised water and ethanol, alternatively, for three times, and then dried at room temperature. The preparation process of the PVA/RGO/MWCNTs nanofibers is depicted in Scheme 1.

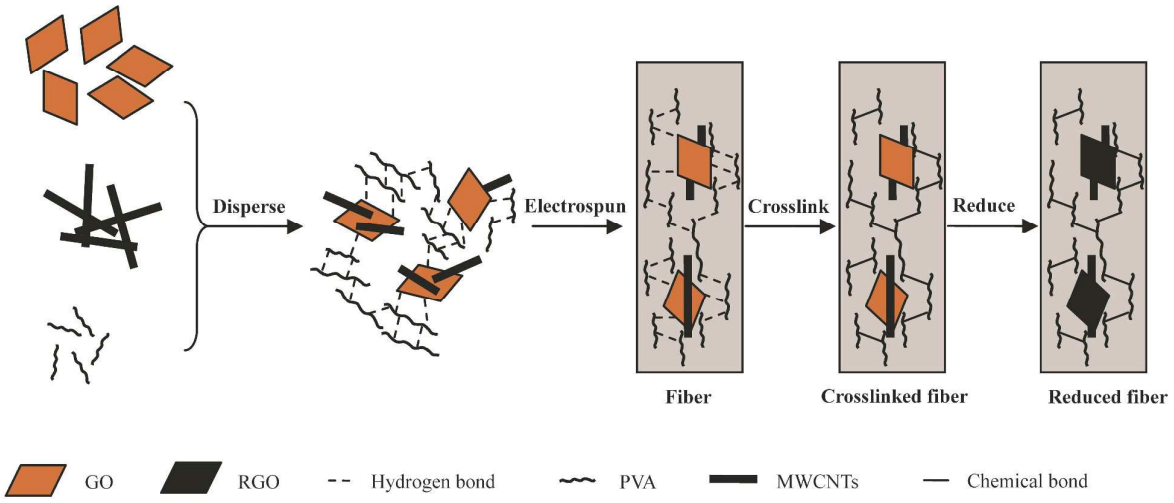

Scheme 1 Schematic process to prepare the PVA/RGO/MWCNTs nanofibers via electrospinning technology and post-treatment of nanofibers

Material characterisation

UV-vis absorption spectra of the electrospinning solutions were measured by a Gold spectrumlab-54 UV-vis spectroscopy in a range of from 200 to 600 nm. Field emission scanning electron microscopy (FESEM) images of the nanofiber mats were recorded on a Hitachi S-4800 with an acceleration voltage of 5.0 kV. The diameters of the nanofibers were analyzed using Software Image J. The dispersion of GO and MWCNTs in nanofibers was recorded on transmission electron microscopy (TEM, JEM-2010UHR, JEOL) with an acceleration voltage of 200 kV. X-ray diffraction (XRD) measurements of the nanofiber mats were conducted on an ARL X'TRA X-ray diffractometer using Cu Kα radiation (λ = 1.5409 Å) at a scanning rate of 10°/min from 5° to 60°. Transmission and attenuated total reflection (ATR) Fourier transform infrared (FTIR) spectra of the uncrosslinked and crosslinked nanofiber mats were obtained with a Nexus 670 spectrometer. The mechanical properties of the nanofiber mats were evaluated by a universal testing machine (E44, MTS Company, Ltd. Shenzhen China) under a crosshead speed 20 mm/min at room temperature. All samples were cut into strips of 30 mm×7mm. At least five samples were tested for each nanofiber mat.

The volume conductivities of the nanofiber mats were evaluated by an insulation resistance (ZC-90E, Sanye Co., Ltd. Shanghai China). At least five samples were tested for each nanofiber mat. All samples were cut into square of 20 mm×20 mm. The samples were pasted conductive adhesive for reducing contact resistance between sample and clip. The two clamping openings were connected with two wires. The volume conductivities were calculated according to the following equation:

$$\sigma = \frac{d}{R \times a \times b}$$

Where σ is the volume conductivity, *a*, *b*, *d* are the length, width, thickness of nanofiber mat, respectively. *R* is the resistance of the nanofiber mat.

Results and discussion

Preparation of the PVA/GO/MWCNTs solution

The stability of electrospinning solution influences significantly morphology of nanofibers. The stability of electrospinning solution depends on dispersion of MWCNTs. However, as a result of the van der Waals force between nanotubes of MWCNTs, MWCNTs aggregates easily and are difficult to disperse uniformly in the electrospinning solution. To enhance the disaggregation of MWCNTs in the electrospinning solution, MWCNTs were dispersed with assistance of GO by ultrasonic treatment. Fig. 1A shows the PVA, PVA/GO, PVA/GO/MWCNTs translucent solutions after dilution of the electrospinning solutions with deionised water. There is not any aggregation and deposit in these solutions. It indicates that GO and GO/MWCNTs are well dispersed in the PVA solution. For the PVA/GO/MWCNTs translucent solution, this may be due to the π-π stacking interaction between MWCNTs and GO. To confirm

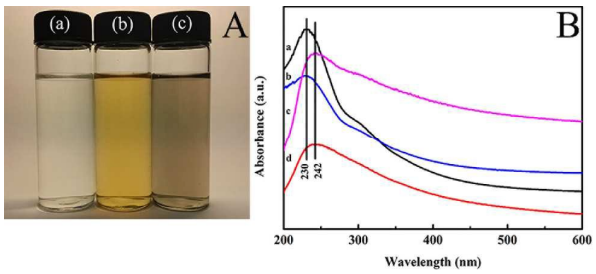

Fig. 1 (A) Digital image of the PVA (a), PVA/GO (b) and PVA/GO/MWCNTs (c) composite solutions after dilution with deionised water; (B) UV-vis absorption spectra of the GO (a), PVA/GO (b), GO/MWCNTs (c) and PVA/GO/MWCNTs (d) solutions

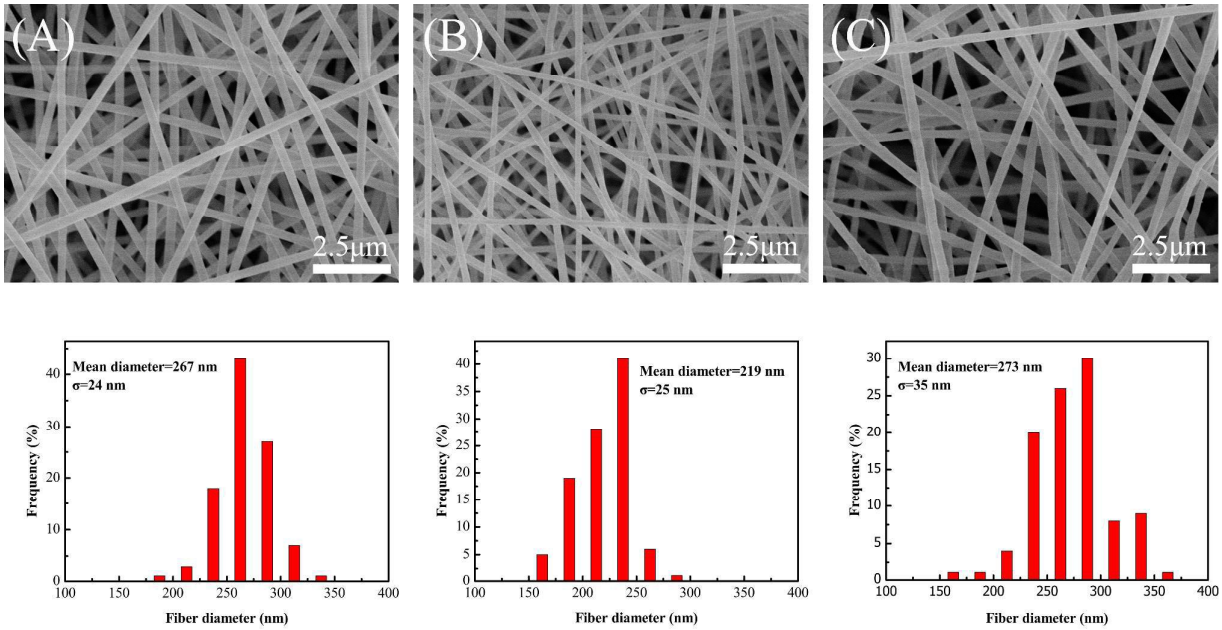

Fig. 2 FESEM images and diameter distribution histograms of the PVA (A), PVA/GO (B) and PVA/GO/MWCNTs (C) nanofiber mats prepared by the electrospinning technology with 13 kV voltages and 15 cm distance

the π-π stacking interaction between MWCNTs and GO in PVA solution, UV-vis absorption spectra of the different solutions were measured (Fig. 1B), the UV-vis absorption peaks of GO (a in Fig. 1B) and PVA/GO (b in Fig. 1B) solutions at 230 nm are assigned to GO. However, the UV-vis absorption peaks of the GO/MWCNTs (c in Fig. 1B) and PVA/GO/MWCNTs (d in Fig. 1B) solutions take red shift from 230 to 242 nm. This is due to each carbon atom from MWCNTs with one nonbonding p-orbital, which could cross cover with the other p-orbital of the non-oxidative carbon atom from GO to form a large π conjugated system.[30, 31] So MWCNTs disperse uniformly in the PVA solution with the assistance of GO. Fortunately, PVA does not affect the formation of the interaction.

Preparation of the nanofiber mats

In order to make sure the optimal addition amounts of GO and MWCNTs in PVA based nanofibers, the nanofibers filled by GO and MWCNTs with different addition amounts were prepared and measured. The detailed preparation is described in ESI†. Fig. S1† shows the FESEM images of the nanofiber mats filled by GO or MWCNTS with different addition amounts. For the electrospun PVA/GO solution, GO in PVA/GO composite solution influences the viscosity of PVA/GO composite solution for electrospinning. The viscosity of PVA/GO composite solution increases with increasing amount of GO.[32] The 10.7 wt% GO-contained composite solution owns a high viscosity, through which, a nanofiber can not be form due to unstable Taylor cone during the processing of electrospinning. However, the viscosity of PVA/GO composite solution is low when the amount of GO is 3.6 wt% or 7 wt%, which is beneficial to the stability of electrospinning. The FESEM images of the 3.6 wt% and 7 wt% GO-filled nanofiber mats show a good morphology of nanofibers. So in order to obtain good dispersion of MWCNTs composite solutions and the stability of electrospinning, 7 wt% GO is the optimal amount of dispersing MWCNTs in this article. The FESEM image of the 14 wt% MWCNTs-filled nanofibers shows the relatively uniform diameter of nanofibers. However, the FESEM image of the 17.9 wt% MWCNTs-filled nanofibers shows many obvious beads due to the agglomeration of MWCNTs. So the 14 wt% MWCNTs is the optimal amount for obtaining good morphology of nanofibers.

Fig. 2 shows the FESEM images and diameter distribution diagrams of the nanofibers prepared from different PVA based solutions via the electrospinning technology. The FESEM images of PVA/GO and PVA/GO/MWCNTs nanofibers show that there is not any bead in nanofibers. It confirms GO and GO/MWCNTs well disperse in PVA based nanofibers. At the same electrospinning conditions, the mean diameter (219 nm) of the PVA/GO nanofibers is smaller than that of the pure PVA nanofibers (267 nm). It is due to that the conductivity of the

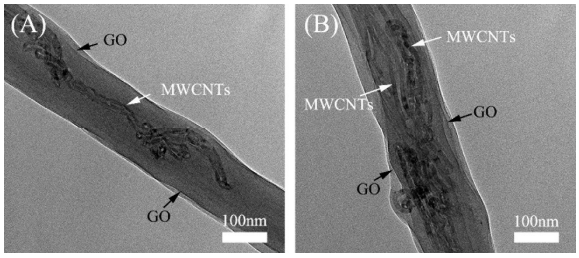

Fig. 3 TEM images of the PVA/GO/MWCNTs nanofibers prepared by the electrospinning technology with 13 kV voltages and 15 cm distance (A) single or (B) multiple MWCNTs disperse in the PVA nanofibers.

PVA/GO solution is improved by GO, which leads to improvement of the net charge density on the surface of jet in the process of electrospinning. The higher net charge density increases the force exerted on the jet, which promotes the stretch of the nanofibers during the process of electrospinning.[33] However, after adding GO, there is no obvious change in the diameter distribution of nanofibers, which may be due to that GO is well dispersed in nanofibers via the hydrogen bonding between GO and PVA.[2] Fig. 2C shows that the PVA/GO/MWCNTs nanofibers own the maximum mean diameter (273 nm) and diameter distribution after addition MWCNTs. The good conductivity of MWCNTs improves the net charge density on the surface of jet, which should lead to the small diameter and narrower diameter distribution of nanofibers.[34] To explain the contradiction, the typical TEM images of PVA/GO/MWCNTs nanofibers were introduced.

Fig. 3 shows the TEM images of the PVA/GO/MWCNTs nanofibers. In the TEM images, GO and MWCNTs are found obviously in the PVA matrix, which confirms that the GO and MWCNTs are localized in the single nanofiber. In the process of electrospinning, the nanotubes of MWCNTs align along the axis of PVA nanofibers. The TEM images show single (A) or multiple (B) MWCNTs and GO disperse well in the PVA nanofibers. For single nanotube dispersed in PVA nanofiber, the increase of conductivity decreases the diameter of nanofiber. For multiple nanotubes dispersed in PVA nanofiber, the multiple nanotubes dispersed in a nanofiber increase the cross section of filler, which increases the diameter of nanofibers. It is why PVA/GO/MWCNTs nanofibers own bigger diameter and wider diameter distribution as shown in the FESEM images (Fig.2C). In addition, the GO nanosheets appear around MWCNTs, which proves that MWCNTs could disperse in nanofibers well with the interaction between them. This result agrees with the result of UV-vis absorption spectra (Fig.1).

Fig. 4 shows the FTIR spectra of the PVA, PVA/GO and PVA/GO/MWCNTS nanofiber mats and GO. In the spectrum of GO (Fig.4a), there are three characteristic peaks at 3430, 1734 and 1229 cm^{-1}, corresponding to —OH stretching vibration of hydroxyl group, C=O stretching vibration of carboxylic group and C-O-C stretching vibration of epoxy group, respectively.[35] However, the peak at 1630 cm^{-1} is attributed to hydroxyl group of water. For PVA nanofiber mat, the peaks at 3353, 2944, and 1734 cm^{-1} are attributed to the —OH stretching vibration, —CH asymmetric stretching vibration and C=O stretching vibration, respectively.[36] In comparison with the —OH stretching peak at 3313 cm^{-1} of the PVA (Fig.4b) nanofiber mat, the peak at 3353 cm^{-1} of the PVA/GO (Fig.4c) and the PVA/GO/MWCNTs (Fig.4d) nanofiber mats shifts to a higher wavenumber. It is due to the formation of hydrogen bond between the oxygen-containing groups of the GO sheets and the hydroxyl groups of the PVA matrix.[3] This is why GO could be well dispersed in PVA solution and PVA nanofiber. So the PVA/GO solution shows translucence after dilution (Fig. 1A). The result agrees with the results of UV-vis absorption spectra (Fig. 1B) and FESEM images (Fig. 2B).

Fig. 5 shows the XRD patterns of the nanofiber mats and the PVA raw materials. For the PVA raw materials, there are four typical peaks at 2θ=11.2°, 19.4°, 22.9°and 40.7°, corresponding to the (100), (101), (111) and (200) reflections of PVA, respectively.[37] However, the peaks at 2θ=11.2°, 22.9°and 40.7° disappear in the PVA nanofiber mat via the electrospinning technology. In comparison with the PVA raw materials, the PVA, PVA/GO, PVA/GO/MWCNTs nanofiber mats all show a relatively weak peak at 19.4°. The reason is

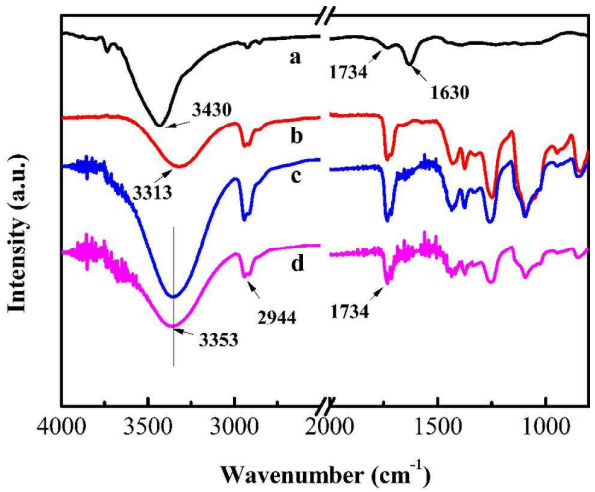

Fig. 4 Transmission FTIR spectra of GO powder (a), the PVA nanofiber mat (b), the PVA/GO nanofiber mat (c) and the PVA/GO/MWCNTS nanofiber mat (d) by the electrospinning technology with 13 kV voltages and 15 cm distance

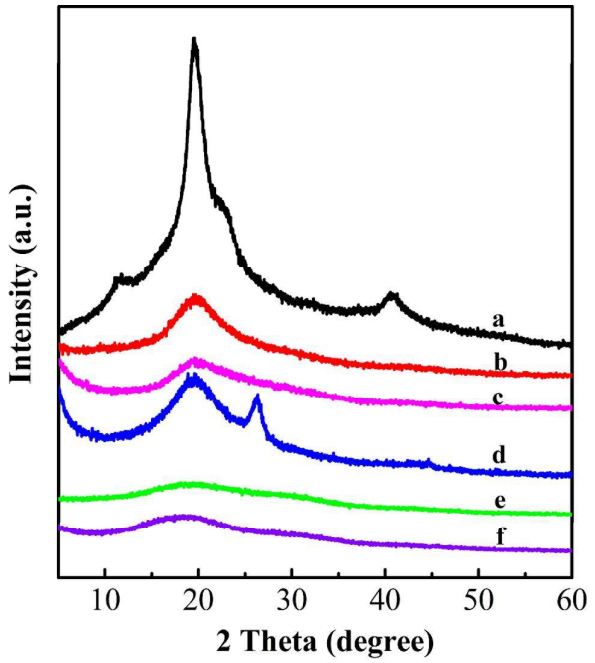

Fig. 5 XRD patterns of PVA raw materials (a), the PVA nanofiber mat (b), the PVA/GO nanofiber mat (c), the PVA/GO/MWCNTs nanofiber mat (d), the crosslinked PVA nanofiber mat (e) and the crosslinked PVA/GO nanofiber mat (f) prepared by the electrospinning technology with 13 kV voltages and 15 cm distance

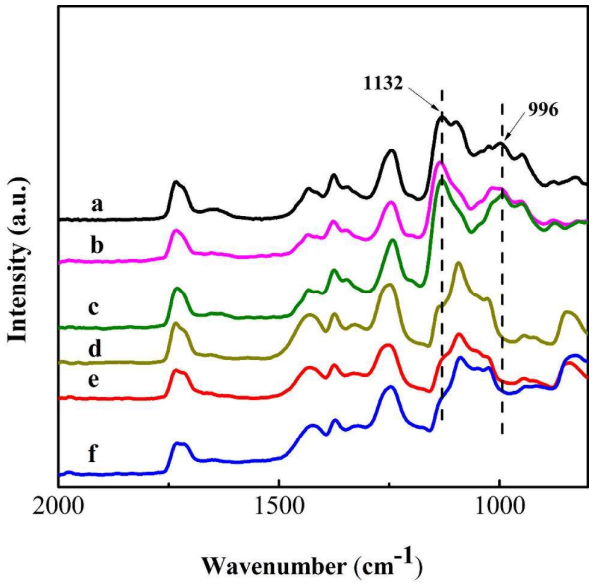

Fig. 6 ATR-FTIR spectra of the PVA (a), PVA/GO (b), PVA/GO/MWCNTs (c) nanofiber mats after crosslinked with GA in methylbenzene (reaction condition pH=2~3) at room temperature for 4 h, the uncrosslinked PVA (d), PVA/GO (e) and PVA/GO/MWCNTs (f) nanofiber mats

that during the electrospinning process, the solution solidified rapidly at high elongation rate so that the molecular chain of PVA could not stretch well, which dramatically diminishes the formation of crystals.[38] By comparison to the PVA nanofiber mat, the PVA/GO nanofiber mat leads to a weaker (101) reflection at 19.4°, which implies that the crystallization of PVA is deteriorated by GO. It might be attributed to the "hydrogen bond barrier" effect of the GO sheets.[39] The GO sheets are well dispersed between PVA chains, which prevents from the formation of the partial hydrogen between PVA chains. So it could significantly hinder the crystallisation of the PVA matrix.[40] Surprisingly, there is no obvious peak of GO exist in the XRD pattern. It is due to that GO nanosheets well disperse between PVA chains with the interaction of hydrogen between GO sheets and PVA chains, which leads the orderliness of GO sheets in nanofibers.[2] After adding MWCNTs, the peak of the PVA/GO/MWCNTs nanofiber mat at 19.4° becomes stronger because MWCNTs promote the nucleation in the process of PVA crystallization.[36] It leads to the higher crystallization capacity of the PVA matrix. It is worth to point out that a new peak at 26.2° is observed in the PVA/GO/MWCNTs nanofiber mat. This peak is attributed to the (002) reflection of MWCNTs.[41] So MWCNTs exist obviously in the PVA/GO/MWCNTs nanofiber mat. For the crosslinked PVA and PVA/GO nanofiber mats, the crosslinked PVA/GO nanofiber mat leads to the almost same strength of (101) reflection at 19.4°. It is due to that the disappearance of hydrogen bond between GO and PVA while the hydroxyl groups are crosslinked by GA. So GO does not influence the crystallization of PVA via "hydrogen bond barrier".

Crosslinking of the nanofiber mats

The PVA based nanofibers are unstable in aqueous solution due to swelling or solubility of PVA molecules. After crosslinking, the crosslinked PVA based nanofibers can be stable in water as well.[42] Hence, GA was used as crosslinking agent for the PVA based nanofiber mats. Fig. 6 shows the ATR-FTIR spectra of these nanofiber mats before and after crosslinked with GA in methylbenzene at pH=2~3. Two new peaks appear obviously at 1132 and 996 cm^{-1}, respectively, after crosslinking. They are attributed to the C-O-C stretching vibration of ether group and the C-O-C-O stretching vibration of acetal group, respectively.[43, 44] Appearance of these peaks derives from the reaction between —OH group from PVA and —CHO group from GA, which proves powerfully to the formation of crosslinked nanofiber mats.

Reduction of GO in the nanofiber mats

Fig. 7 shows the Raman spectra of GO and the PVA/GO nanofiber mat before and after reduced by hydrazine hydrate at 95 °C for 1 h. Two obvious peaks at 1348 and 1583 cm^{-1} exist in the spectra, which are attributed to D band and G band of carbon, respectively. The D band corresponding to a breathing mode of *k*-point photons of A_{1g} symmetry and the G band corresponding to the first-order scattering of the E_{2g} mode derives from sp^3 and sp^2 carbon domains, respectively.[45] The change of I_D/I_G value (intensity ratio of D and G bands) can prove the degree of reduction.[46] After reduction by hydrazine hydrate, the I_D/I_G value of GO increases from 0.83 to 1.07, the I_D/I_G value of the PVA/GO nanofiber mat increases from 0.83 to 1.11. These indicate the reduction of GO into RGO does take place.[47] The increasing of I_D/I_G ratio after reduction of GO is due to the formation of new graphitic domains which owns smaller the average size of the sp^2 domains than GO, but more numerous in number.[48] To further prove the reduction of GO, UV-vis absorption spectra of the GO and RGO solutions and the suspension solution of PVA/RGO nanofiber mats were measured. Firstly, the PVA/RGO nanofiber mat was crushed in a mortar. Secondly, the crushed nanofiber mat was dispersed in deionised water with ultrasonic treatment. So the suspension solution of PVA/RGO nanofiber mat was obtained. Fig. 8 shows the UV-vis spectra of PVA/RGO nanofiber mat suspension solution and GO solution before and after reduced by hydrazine hydrate at 95 °C for 1 h. The absorption peak of GO at 230 nm takes red shift to 265 nm. It indicates that GO

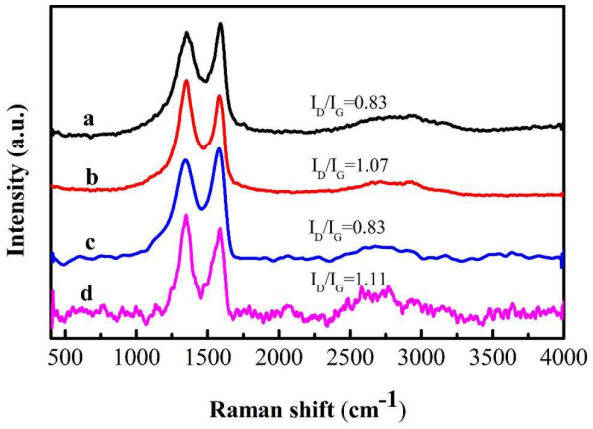

Fig.7 Raman spectra of GO before (a) and after (c) reduced by hydrazine hydrate at 95 °C for 1 h, the PVA/GO nanofiber mat before (c) and after (d) reduced by hydrazine hydrate at 95 °C for 1 h

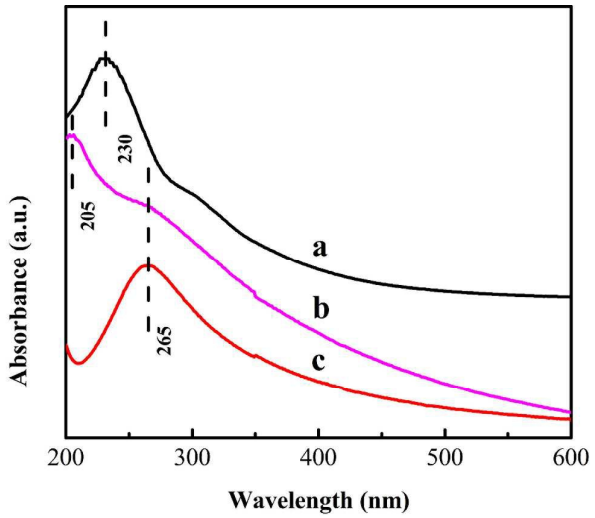

Fig. 8 UV-vis absorption spectra of the GO (a) solution, PVA/RGO (b) solution after crush and ultrasonic treatment of the PVA/RGO nanofiber mat in deionised water and the RGO solution (c)

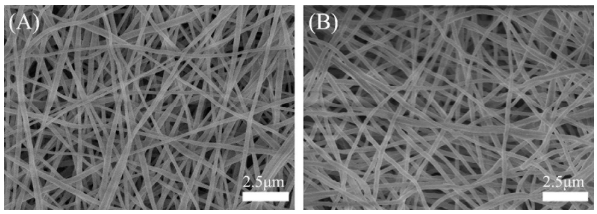

Fig.9 FESEM images of the PVA/RGO (A) and PVA/RGO/MWCNTs (B) nanofiber mats prepared via reduction of the PVA/RGO and PVA/RGO/MWCNTs nanofiber mats in hydrazine hydrate at 95 ^{o}C for 1 h, respectively

might be reduced.[49] The obvious peak at 205 nm of the PVA/RGO nanofiber mat suspension solution might be due to the π-π attraction between RGO and RGO fragments.[21] These fragments might be originated from the process of crush and ultrasonic treatment.

Fig. 9 shows the FESEM images of the PVA/RGO and PVA/RGO/MWCNTs nanofiber mats. It can be observed that these nanofibers maintain original morphology after crosslinked with GA and reduced with hydrazine hydrate aqueous solution at 95 ^{o}C for 1 h. The result also shows the stability of the crosslinked PVA based nanofiber mats in aqueous solution at 95 ^{o}C, which proves further the formation of crosslinked PVA based nanofiber mats.

Fig.10 shows digital image of the different nanofiber mats. The PVA (A1 in Fig. 10), PVA/GO (B1 in Fig. 10), PVA/GO/MWCNTs (C1 in Fig. 10) nanofiber mats show obviously different colour. The colour of nanofiber mat transferred from white (A1 in Fig. 10) to brown (B1 in Fig. 10) with addition of GO. However, the PVA/GO/MWCNTs nanofiber mat (C1 in Fig. 10) shows black. These uniform colours of the PVA/GO and PVA/GO/MWCNTs nanofiber mats confirm that GO and GO/MWCNTs are uniformly dispersed in PVA based nanofibers. It agrees with these results of Figs. 1–3. There are no obviously changes of colour before and after crosslinking of the PVA, PVA/GO, PVA/GO/MWCNTs nanofiber mats, which confirms that GO and MWCNTs in nanofibers do not change before and after crosslinking except for formation of the crosslinked network. Differently, after treatment with hydrazine hydrate, colour of the PVA/GO nanofiber mat transfers from brown (B2 in Fig. 10) to black (B3 in Fig. 10) due to blackness of RGO derived from GO after reduction. The PVA/GO/MWCNTs nanofiber mat (C3 in Fig. 10) shows the blackest colour, which is attributed to the highest carbon (RGO and MWCNTs) content in nanofibers.

Properties of the nanofiber mats

Fig. 11 shows the stress-strain curves of the different nanofiber mats. Before and after crosslinked, the Young's modulus of all the nanofiber mats increase gradually with the added nanofiller (GO, GO/MWCNTs). And the crosslinked nanofiber mats own higher Young's modulus. Before crosslinked, the PVA nanofiber mat owns the largest elongation-at-break. It is because the good movement of the PVA chains. After addition of GO, the hydrogen bonding between GO and PVA restricts the movement of the PVA chains.[50] So the PVA/GO nanofiber mat owns lower elongation-at-break. The elongation-at-break of the PVA/GO/MWCNTs nanofiber mat is higher than that of the PVA/GO nanofiber mat. It is attributed to the well dispersion of MWCNTs.[51, 52] After crosslinked, the formative chemical bonds between the PVA chains restrict greatly the movement of the PVA chains. Moreover, hydrogen bond disappears in all PVA based nanofiber mats while the hydroxyl groups are crosslinked by GA. So their elongation-at-breaks of crosslinked are almost same.

Fig. 12 shows the tensile strength of the different nanofiber mats before and after crosslinked by GA. For the uncrosslinked nanofiber mats, the tensile strength of the PVA nanofiber mat is 16.7±0.7 MPa. After addition of GO, the tensile strength of the PVA nanofiber mat decreases from 16.7±0.7 to 13.2±0.8 MPa. Although the GO sheets can be favourable to load transfer from polymer matrix to GO,[2] the crystallinity of the PVA matrix in PVA/GO nanofiber mat is lower than that of the PVA nanofiber mat as shown in Fig. 5. It is because that the "hydrogen bond barrier" prevents from the formation of the hydrogen bond between PVA chains. So it could reduce the crystallinity of the PVA matrix. The results agree with the results of XRD patterns. However, some papers have reported the tensile strength of PVA/GO nanofibers is higher than that of PVA nanofibers only when the content of GO is lower than a critical value (0.4~1 wt%).[2, 53] When the content of GO is higher than the critical value, the tensile strength of PVA/GO nanofibers decreases gradually. The variation is due to that effect of "hydrogen bond barrier" on crystallization is very weak in the PVA/GO nanofiber with low content of GO as reported in the reference.[2, 53] And the GO sheets can be favourable to load transfer from polymer matrix to the GO sheets. When the content of GO is higher than the critical value, the influence of "hydrogen bond barrier" begins to become remarkable, which decreases the formation of the

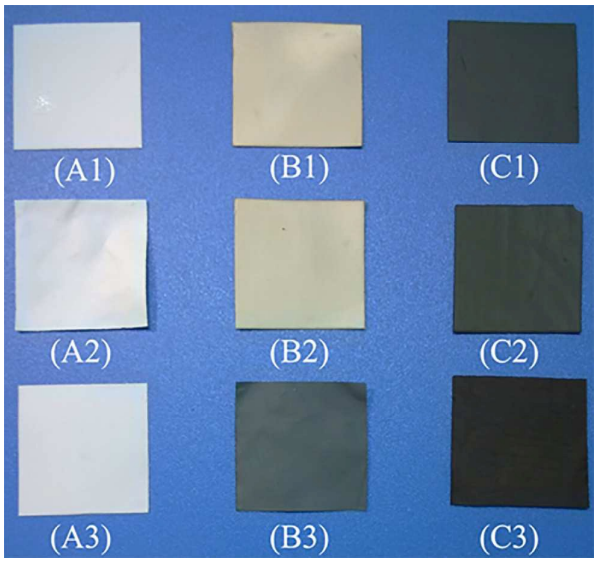

Fig. 10 Digital image of the PVA (A1), PVA/GO (B1) and PVA/GO/MWCNTs (C1) nanofiber mats; the PVA (A2), PVA/GO (B2) and PVA/GO/MWCNTs (C2) nanofiber mats crosslinked with GA in methylbenzene (pH=2~3, adjusted by HCl) at room temperature for 4 h; the reduced PVA (A3), PVA/GO (B3), PVA/GO/MWCNTs (C3) nanofiber mats with hydrazine hydrate at 95 °C for 1 h

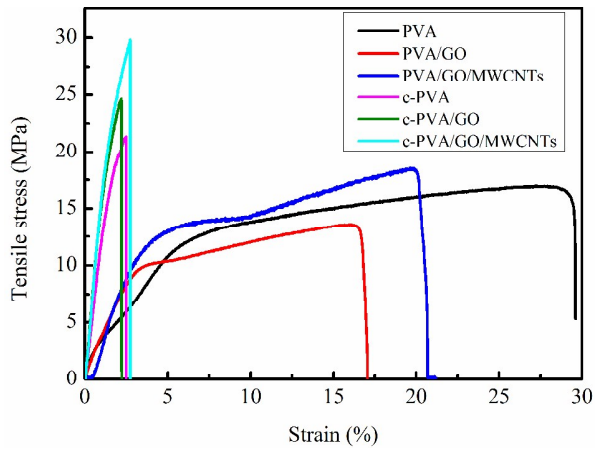

Fig. 11 Stress–strain curves of the PVA, PVA/GO, PVA/GO/MWCNTs, crosslinked PVA (c-PVA), crosslinked PVA/GO (c-PVA/GO) and crosslinked PVA/GO/MWCNTs (c-PVA/GO/MWCNTs) nanofiber mats

hydrogen bond between PVA chains. It could reduce the crystallinity of the PVA matrix. So the tensile strength of PVA/GO nanofibers is higher than that of PVA nanofibers in this case. In this article, 7 wt% GO was filled in the PVA based nanofibers. The amount of GO is much higher than the critical value. So the tensile strength of PVA/GO nanofibers is lower than that of the PVA nanofibers in this article. Before crosslinked, the PVA/GO/MWCNTs nanofiber mat owns the maximum tensile strength (18.1±0.5 MPa). The reason is that the existing MWCNTs promote the crystallization of the PVA matrix as shown in Fig. 5d. At the same time, the well dispersion MWCNTs promotes the load transfer during the mechanical test. For the crosslinked nanofiber mats, GO does not influence the crystallization of PVA via "hydrogen bond

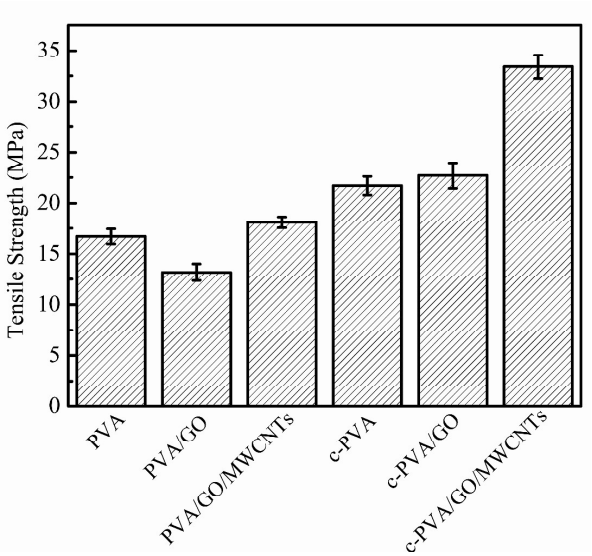

Fig. 12 Tensile strength of the uncrosslinked PVA, PVA/GO, PVA/GO/MWCNTs nanofiber mats and the crosslinked PVA, PVA/GO, PVA/GO/MWCNTs nanofiber mats with GA, respectively (i.e. c-PVA, c-PVA/GO and PVA/GO/MWCNTs)

barrier" because almost all the –OH groups in PVA matrix have disappeared after reacting with –CHO of GA during the crosslinking reaction. [54] The result agrees with the results of XRD patterns (Fig.5). So the crosslinked PVA/GO nanofiber mat has a higher tensile strength than the crosslinked PVA nanofiber mat because of the load transfer from PVA matrix to GO sheets. It is worthy to note that the uncrosslinked nanofiber mats have lower tensile strength than those crosslinked ones. So the nanofiber mats crosslinked with GA own higher mechanical strength. In comparison with the uncrosslinked PVA nanofiber mat (in table S1†), the tensile strength of the crosslinked PVA nanofiber mat improves 30%. The improvement of tensile strength is due to the formation of the crosslinking network. The tensile strengths of the PVA/GO and PVA/GO/MWNTs nanofiber before and after crosslinked have a large variation. It is because that the influence of "hydrogen bond barrier" disappears after that hydroxyl groups are crosslinked. However, the enhance degree of the tensile strengths is no obviously different for the PVA/GO and PVA/GO/MWCNTs nanofiber mats before and after crosslinked. The little difference may be due to the different amount of filler.

Table 1 shows volume conductivities of the different nanofiber mats. The pure PVA nanofiber mat has the lowest volume conductivity ($5.11\pm0.96\times10^{-11}$ S/m). After addition of GO, the volume conductivity of the PVA/GO nanofiber mat increases to $1.27\pm0.71\times10^{-10}$ S/m. It is due to conductivity of GO which improves the volume conductivity of the PVA/GO nanofiber mat. It is worthy to point out that the PVA/RGO nanofiber mat owns slightly higher volume conductivity than the PVA/GO/MWCNTs nanofiber mat although the PVA/GO/MWCNTs nanofiber mat owns higher carbon content than the PVA/RGO nanofiber mat. It is because that GO has a lower conductivity than MWCNTs and GO exists around MWCNTs in nanofibers as shown in Fig. 3, which limits

Table 1 Volume conductivity of the PVA, PVA/GO, PVA/GO/MWCNTs, PVA/RGO, PVA/RGO/MWCNTs nanofiber mats

Nanofiber mats	GO/PVA (%w/w)	MWCNTs/PVA (%w/w)	RGO/PVA (%w/w)	Volume conductivity (S/m)
PVA	—	—	—	$5.11\pm0.96\times10^{-11}$
PVA/GO	7	—	—	$1.27\pm0.71\times10^{-10}$
PVA/GO/MWCNTs	7	14	—	$1.49\pm0.63\times10^{-8}$
PVA/RGO	—	—	7	$3.92\pm0.17\times10^{-8}$
PVA/RGO/MWCNTs	—	14	7	$2.33\pm0.20\times10^{-7}$

conductivity of MWCNTs greatly. After the PVA/GO nanofiber mat was reduced by hydrazine hydrate, GO transfers into RGO. RGO has a higher conductivity than GO.[55, 56] So the PVA/RGO/MWCNTs nanofiber mat has the highest volume conductivity ($2.33\pm0.20\times10^{-7}$ S/m) because the PVA/RGO/MWCNTs nanofiber mat owns the highest carbon content (21 wt%) after reduction of GO.

Conclusions

The PVA/GO/MWCNTs nanofiber mat was fabricated successfully with GO-assisted dispersion of MWCNTs through electrospinning technology. MWCNTs were dispersed well in PVA matrix with assistance of GO. In order to increase the volume conductivity of the PVA/GO/MWCNTs nanofiber mat, GO in nanofibers was reduced by hydrazine hydrate. So the obtained PVA/RGO/MWCNTs nanofiber mat containing the highest content of carbon (21 wt%) has the highest volume conductivity ($2.33\pm0.20\times10^{-7}$ S/m). The crosslinking not only maintains the nanofiber morphology of nanofibers during the process of reduction, but also increases the tensile strength of the nanofiber mats. At the same time, the crosslinked nanofibers can be stable in aqueous solution. The method of improving the carbon content in nanofibers reported here solves the problem of the agglomeration of MWCNTs in nanofibers and improves the carbon content in nanofibers. Our work provides the novel method to prepare the stable aqueous MWCNTs based solution with good dispersion and the highly conductive MWCNTs base nanofibers with high carbon content.

Acknowledgements

This work was funded by the Nature Science Foundation of China (No.50802042), the Nature Science Foundation of Jiangsu province (No. BK2011076) and the Priority Academic Program Development of Jiangsu Higher Education Institutions (PAPD).

References

1. L. Jin, Z. Q. Feng, T. Wang, Z. Z. Ren, S. S. Ma, J. H. Wu and D. P. Sun, *Journal of Materials Chemistry B*, 2014, **2**, 129-136.
2. Y. Y. Qi, Z. X. Tai, D. F. Sun, J. T. Chen, H. B. Ma, X. B. Yan, B. Liu and Q. J. Xue, *Journal of Applied Polymer Science*, 2013, **127**, 1885-1894.
3. X. H. Li, W. M. Yang, H. Y. Li, Y. Wang, M. M. Bubakir, Y. M. Ding and Y. C. Zhang, *Journal of Applied Polymer Science*, 2015, **132**, 41601.
4. A. M. Al-Enizi, A. A. Elzatahry, A. R. I. Soliman and S. S. Al-Theyab, *International Journal of Electrochemical Science*, 2012, **7**, 12646-12655.
5. Y. Fu, L. Liu, L. Q. Zhang and W. C. Wang, *ACS Applied Materials & Interfaces*, 2014, **6**, 5105-5112.
6. M. Yang, T. Xie, L. Peng, Y. Zhao and D. Wang, *Applied Physics A-Materials Science & Processing*, 2007, **89**, 427-430.
7. I. D. Norris, M. M. Shaker, F. K. Ko and A. G. MacDiarmid, *Synthetic Metals*, 2000, **114**, 109-114.
8. E. T. Thostenson, Z. F. Ren and T. W. Chou, *Composites Science and Technology*, 2001, **61**, 1899-1912.
9. H. Liu, K. C. Zuo and C. D. Vecitis, *Environmental Science & Technology*, 2014, **48**, 13871-13879.
10. H. Ko, S. Park, S. Park and C. Lee, *Journal of Nanoscience and Nanotechnology*, 2015, **15**, 5295-5300.
11. H. Huang, C. H. Liu, Y. Wu and S. S. Fan, *Advanced Materials*, 2005, **17**, 1652-1656.
12. M. Foldvari and M. Bagonluri, *Nanomedicine-Nanotechnology Biology and Medicine*, 2008, **4**, 183-200.
13. G. Salimbeygi, K. Nasouri and A. M. Shoushtari, *Fibers and Polymers*, 2014, **15**, 583-588.
14. J. S. Jeong, J. S. Moon, S. Y. Jeon, J. H. Park, P. S. Alegaonkar and J. B. Yoo, *Thin Solid Films*, 2007, **515**, 5136-5141.
15. Z. Q. Ding, Y. P. Zhu, C. Branford-White, K. Sun, S. Um-I-Zahra, J. Quan, H. L. Nie and L. M. Zhu, *Materials Letters*, 2014, **128**, 310-313.
16. W. B. Lu, B. Liu, J. Wu, J. Xiao, K. C. Hwang, S. Y. Fu and Y. Huang, *Applied Physics Letters*, 2009, **94**, 101917.
17. P. Abadi, M. R. Maschmann, S. M. Mortuza, S. Banerjee, J. W. Baur, S. Graham and B. A. Cola, *Carbon*, 2014, **69**, 178-187.
18. B. Kim and W. M. Sigmund, *Langmuir*, 2004, **20**, 8239-8242.
19. Y. B. Wang, Z. Iqbal and S. Mitra, *Journal of the American Chemical Society*, 2006, **128**, 95-99.
20. M. J. Kim, J. Lee, D. Jung and S. E. Shim, *Synthetic Metals*, 2010, **160**, 1410-1414.
21. J. Kim, L. J. Cote, F. Kim, W. Yuan, K. R. Shull and J. X. Huang, *Journal of the American Chemical Society*, 2010, **132**, 8180-8186.
22. V. C. Tung, J. H. Huang, I. Tevis, F. Kim, J. Kim, C. W. Chu, S. I. Stupp and J. X. Huang, *Journal of the American Chemical Society*, 2011, **133**, 4940-4947.
23. S. H. Aboutalebi, A. T. Chidembo, M. Salari, K. Konstantinov, D. Wexler, H. K. Liu and S. X. Dou, *Energy & Environmental Science*, 2011, **4**, 1855-1865.

24. J. Ma, L. Zhou, C. Li, J. H. Yang, T. Meng, H. M. Zhou, M. X. Yang, F. Yu and J. H. Chen, *Journal of Power Sources*, 2014, **247**, 999-1004.
25. L. Qiu, X. W. Yang, X. L. Gou, W. R. Yang, Z. F. Ma, G. G. Wallace and D. Li, *Chemistry-A European Journal*, 2010, **16**, 10653-10658.
26. D. Chen, H. B. Feng and J. H. Li, *Chemical Reviews*, 2012, **112**, 6027-6053.
27. S. K. Pillai, S. S. Ray and M. Moodley, *Journal of Nanoscience and Nanotechnology*, 2008, **8**, 6187-6207.
28. O. Koysuren, *Journal of Polymer Engineering*, 2012, **32**, 407-413.
29. W. P. Zhou, Y. L. Wu, F. Wei, G. H. Luo and W. Z. Qian, *Polymer*, 2005, **46**, 12689-12695.
30. V. Mani, S. M. Chen and B. S. Lou, *International Journal of Electrochemical Science*, 2013, **8**, 11641-11660.
31. C. Zhang, S. Huang, W. W. Tjiu, W. Fan and T. X. Liu, *Journal of Materials Chemistry*, 2012, **22**, 2427-2434.
32. Y. Tan, Y. Song and Q. Zheng, *Nanoscale*, 2012, **4**, 6997-7005.
33. H. Fong, I. Chun and D. H. Reneker, *Polymer*, 1999, **40**, 4585-4592.
34. H. Bang, M. Gopiraman, B. S. Kim, S. H. Kim and I.S. Kim, *Colloids and Surfaces A-Physicochemical and Engineering Aspects*, 2012, **409**, 112-117.
35. M. Srivastava, M. E. Uddin, J. Singh, N. H. Kim and J. H. Lee, *Journal of Alloys and Compounds*, 2014, **590**, 266-276.
36. M. Naebe, T. Lin, W. Tian, L. M. Dai and X. G. Wang, *Nanotechnology*, 2007, **18**, 225605.
37. L. M. Guerrini, M. P. de Oliveira, M. C. Branciforti, T. A. Custodio and R. E. S. Bretas, *Journal of Applied Polymer Science*, 2009, **112**, 1680-1687.
38. Y. S. Zhou, H. J. Yang, X. Liu, J. Mao, S. J. Gu and W. L. Xu, *International Journal of Biological Macromolecules*, 2013, **53**, 88-92.
39. C. Bao, Y. Guo, L. Song and Y. Hu, *Journal of Materials Chemistry*, 2011, **21**, 13942-13950.
40. J. J. Li, L. S. Shao, X. H. Zhou and Y. H. Wang, *RSC Advances*, 2014, **4**, 43612-43618.
41. T. Ohta, T. Ito, M. Shimizu, L. Tauchi, H. D. Nguyen-Tran, J. C. Park, B. S. Kim, I. S. Kim and K. Ohta, *Polymers for Advanced Technologies*, 2011, **22**, 2653-2658.
42. A. G. Destaye, C. K. Lin and C. K. Lee, *ACS Applied Materials & Interfaces*, 2013, **5**, 4745-4752.
43. R. P. Shaikh, P. Kumar, Y. E. Choonara, L. C. du Toit and V. Pillay, *Biofabrication*, 2012, **4**, 025002.
44. R. Guo, C. Hu, B. Li and Z. Jiang, *Journal of Membrane Science*, 2007, **289**, 191-198.
45. X. F. Li, J. F. Shen, N. Li and M. X. Ye, *Journal of Power Sources*, 2015, **282**, 194-201.
46. J. L. Zhang, H. J. Yang, G. X. Shen, P. Cheng, J. Y. Zhang and S. W. Guo, *Chemical Communications*, 2010, **46**, 1112-1114.
47. X. D. Qi, X. L. Yao, S. Deng, T. N. Zhou and Q. Fu, *Journal of Materials Chemistry A*, 2014, **2**, 2240-2249.
48. S. Stankovich, D. A. Dikin, R. D. Piner, K. A. Kohlhaas, A. Kleinhammes, Y. Jia, Y. Wu, S. T. Nguyen and R. S. Ruoff, *Carbon*, 2007, **45**, 1558-1565.
49. D. Li, M. B. Muller, S. Gilje, R. B. Kaner and G. G. Wallace, *Nature Nanotechnology*, 2008, **3**, 101-105.
50. C. Wang, Y. Li, G. Ding, X. Xie and M. Jiang, *Journal of Applied Polymer Science*, 2013, **127**, 3026-3032.
51. D. Chen, R. Y. Wang, W. W. Tjiu and T. X. Liu, *Composites Science and Technology*, 2011, **71**, 1556-1562.
52. L. D. Tijing, W. Choi, Z. Jiang, A. Amarjargal, C. H. Park, H. R. Pant, I. T. Im and C. S. Kim, *Current Applied Physics*, 2013, **13**, 1247-1255.
53. Y. Liu, M. Park, H. K. Shin, B. Pant, J. Choi, Y. W. Park, J. Y. Lee, S.-J. Park and H.-Y. Kim, *Journal of Industrial and Engineering Chemistry*, 2014, **20**, 4415-4420.
54. H. S. Mansur, R. L. Orefice and A. A. P. Mansur, *Polymer*, 2004, **45**, 7193-7202.
55. R. H. Wang, Y. Wang, C. H. Xu, J. Sun and L. Gao, *RSC Advances*, 2013, **3**, 1194-1200.
56. Y. Wang, L. Chen, J. R. Yu, J. Zhu, Z. X. Shi and Z. M. Hu, *RSC Advances*, 2013, **3**, 12255-12266.